Use of graphene as an additive to improve the mechanical properties of gypsum plaster

Uso do grafeno como aditivo para melhorar as propriedades mecânicas do gesso

DOI:10.34117/bjdv9n5-049

Recebimento dos originais: 04/04/2023
Aceitação para publicação: 05/05/2023

Adller Ernesto de Lima Ferreira
Master in Materials Science and Technology
Institution: Universidade Federal do Triângulo Mineiro (UFTM)
Address Avenida Doutor Randolfo Borges Júnior, Minas Gerais, Brasil
E-mail: adllerernesto@hotmail.com

Felipe Silva Lima
Graduated in Civil Engineering
Institution: Universidade Federal do Triângulo Mineiro (UFTM)
Address Avenida Doutor Randolfo Borges Júnior, Minas Gerais, Brasil
E-mail: felipe_silvalima@hotmail.com

João Pedro Lopes do Nascimento
Master in Agrochemistry
Institution: Universidade Federal do Triângulo Mineiro (UFTM)
Address Avenida Doutor Randolfo Borges Júnior, Minas Gerais, Brasil
E-mail: jpl.nascimento@outlook.com

Paulo de Castro Guetti
PhD in Structural Engineering
Institution: Universidade Federal do Triângulo Mineiro (UFTM)
Address Avenida Doutor Randolfo Borges Júnior, Minas Gerais, Brasil
E-mail: guettipc@gmail.com

Mario Sérgio da Luz
PhD in Materials Engineering
Institution: Universidade Federal do Triângulo Mineiro (UFTM)
Address Avenida Doutor Randolfo Borges Júnior, Minas Gerais, Brasil
E-mail: mario.luz@uftm.edu.br

Jéferson Aparecido Moreto
PhD in Materials Science & Engineering
Institution: Universidade Federal do Triângulo Mineiro (UFTM)
Address Avenida Doutor Randolfo Borges Júnior, Minas Gerais, Brasil
E-mail: jeferson.moreto@uftm.edu.br

Rogério Valentim Gelamo
PhD in Physics
Institution: Universidade Federal do Triângulo Mineiro (UFTM)
Address Avenida Doutor Randolfo Borges Júnior, Minas Gerais, Brasil
E-mail: rogelamo@gmail.com

ABSTRACT
This work aimed to investigate the effects of graphene nanoparticles on the mechanical and morphological properties of gypsum plaster paste. In order to do so, samples of pure gypsum plaster paste with multilayer graphene were produced. These samples were prepared with a water/plaster factor (w/p) of approximately 0.5 with different graphene dosages. The mechanical analysis results showed that the graphene dosage of 0.02% increased the compressive and tensile strength values in the order of 120%. The increase in these properties is most likely due to the heat dissipation promoted by graphene, the greater production of crystalline nuclei and the reactivity of graphene with Ca2+ ions. Regarding the plaster setting times, a reduction in the values was observed for most samples, indicating an increase in the production of crystalline nuclei. FTIR analyzes indicate that there were no changes in terms of chemical properties.

Keywords: plaster, gypsum, graphene, composite, mechanical properties.

RESUMO
Este trabalho teve como objetivo investigar os efeitos de nanopartículas de grafeno nas propriedades mecânicas e morfológicas da pasta de gesso. Para isso, foram produzidas amostras de pasta de gesso puro com grafeno multicamadas, preparadas com um fator água/gesso (w/p) de aproximadamente 0,5 e diferentes dosagens de grafeno. Os resultados dos testes mecânicos mostraram que a dosagem de 0,02% de grafeno aumentou os valores de resistência à compressão e tração em até 120%. O aumento dessas propriedades provavelmente se deve à dissipação de calor promovida pelo grafeno, a maior produção de núcleos cristalinos e à reatividade do grafeno com os íons Ca^{2+}. Com relação aos tempos de presa do gesso, observou-se redução dos valores para a maioria das amostras, indicando aumento na produção de núcleos cristalinos. As análises de FTIR indicam que não houve alterações em termos de propriedades químicas.

Palavras-chave: argamassa, gesso, grafeno, compósito, propriedades mecânicas.

1 INTRODUCTION

Gypsum plaster has been widely used in civil construction as pre-molded boards (drywall), sealing blocks, coatings, grouts, restoration of ancients finishes and details such as crown molding and three-dimensional plates (FREIRE et al., 2021). Among the many advantages that gypsum plaster presents, it is possible to highlight its lightness, practicality, application speed and very low cost when compared to conventional sealing and coating systems. In addition, drywall building materials can be up to 7 times lighter than ceramic block walls, which allows for the design of slenderer structures and

foundations, generating savings in cement and steel consumption, which means less environmental impact (BORRACHERO et al., 2008). Considering that the cement production process is responsible for more than 6% of all CO_2 emitted worldwide (ISAIA; GASTALDINI, 2004), the use of gypsum plaster in the civil construction area appears as a possibility to reduce the environmental impact.

Gypsum plaster is a material mainly produced from the calcination of the mineral gypsum, a process in which the raw material (calcium sulfate dihydrate – $CaSO_4.2H_2O$) is pulverized and subjected to temperatures close to 140 ºC, releasing water vapor into the environment and giving rise to commercial gypsum plaster (calcium sulfate hemihydrate – $CaSO_4.\ 1/2H_2O$) (BALTAR; BASTOS; LUIZ, DA, 2008). The hardening process (rehydration) takes place after mixing the plaster with water. During this time the plaster temporarily becomes plastic and, during the drying process, returns to its original form (dihydrate). Thus, it is a reversible process as long as the chemical bonds of its crystals are broken, and the material is decontaminated. This process has been an object of study in recycling (GERALDO et al., 2017). These above-mentioned characteristics give the plaster interesting sustainable and recyclable potential. However, despite the advantages, its fragility and water intolerance discourage its use.

The hydration reaction of gypsum plaster is exothermic, releasing a large amount of energy in the form of heat. However, it has low thermal conductivity (KORTE; BROUWERS, 2010) and as the hydration reactions occur, heat accumulates in central regions of the paste, promoting different crystallization conditions between the central and peripheral regions of the sample. Thus, the energy released alters the plaster's solubility, influencing the hydration kinetics (CHAROLA; PÜHRINGER; STEIGER, 2007; HULETT; ALLEN, 1902), crystallographic density and the material's mechanical performance. In other words, it can be considered that the relationship between temperature and solubility negatively alters the crystalline homogeneity, promoting the formation of crystals of different sizes and densities. In order to improve the specific plaster properties, such as water absorption, adhesiveness, and setting time, chemical additives are usually used (BALTAR; BASTOS; LUIZ, DA, 2008). Recent studies show the influence of cellulose fibers (ROSATO et al., 2017; SENFF et al., 2018), TiO_2 nanoparticulate systems (ROSATO et al., 2017), expanded polystyrene, and carbonate and silica minerals (PERLOVA et al., 2016) on gypsum plaster's mechanical properties. The literature (GONG et al., 2015; MORSY; ALSAYED; AQEL, 2011; SILVA et al., 2017) reported the result of incorporating carbon-based nanoparticles in ceramic binders,

revealing an increase in their mechanical strength and in the optimization of their electrical and thermal properties (CHUNG, 2012; HOU et al., 2019).

Nanostructured systems based on multilayer graphene (MLG) have extraordinary properties, such as high tensile and compressive strength, and high thermal and electrical conductivities (CHEN; TANG; LI, 2010; LEE et al., 2008; WEI; QU, 2012). For this reason, graphene has been studied in Physics, Chemistry, Materials Science and Engineering, Medicine, etc. (BROWNSON; KAMPOURIS; BANKS, 2012; LOTA et al., 2008; NOVOSELOV et al., 2004). Furthermore, research shows that the incorporation of MLG in ceramic matrices generates changes in crystallization mechanisms, producing denser cores and more mechanically resistant and durable mortars.

As reported by Silva et al. (2017) and Gdoutos (2016), incorporating nanostructured systems, such as nanofibers, carbon nanotubes and multilayer graphene, considerably optimizes the mechanical strength of cementitious composites. However, using multilayer graphene in systems that receive water as a catalyst is quite challenging. This is due to the fact that graphene displays hydrophobic behavior, which makes its dispersion difficult and promotes a tendency to agglomerate. The agglomeration process is probably due to the interaction between the multilayers by Van der Waals forces (PARVEEN; RANA; FANGUEIRO, 2013). The use of surfactants appears as an alternative for the optimization of dispersion; however, they negatively affect the material's elastic modulus and tensile strength (PAPAGEORGIOU; KINLOCH; YOUNG, 2015). Jara et al. (2021) investigated the effects of incorporating graphene in gypsum mortar at concentrations of 0, 0.05, 0.08 and 0.1% by weight and observed better results with mechanical tests (bending strength) for the sample with the highest concentration of graphene, resulting in an improvement of 22.4 % in relation to the sample without graphene. However, there is no information about the structural, morphological, or other properties of the samples they studied.

In this study, we proposed to carry out innovative and applied research to study the influence of MLG on the mechanical properties of gypsum plaster. The system was characterized morphologically and structurally via scanning electron microscopy (SEM), optical microscopy (OM), Fourier transform infrared spectroscopy (FTIR) and X-ray diffraction (XRD). It was also the aim of this study to verify the consistency of the plaster containing MLG and setting start and end times by means of Vicat tests. The resistance of gypsum plaster containing MLG to water was verified via mass loss analysis after the submersion process.

2 EXPERIMENTAL

2.1 MATERIALS

In the present work, β-type gypsum plaster with a fineness modulus of 1.11, a unit mass of 713.06 kg/m³ and multilayer graphene (MLG) was used. The MLG samples used in this study were obtained by exfoliating natural graphite flakes donated by the company Nacional de Grafite Ltda. Further details about this procedure used can be seen in the references (MACHUNO et al., 2015). The specimens have thicknesses from 1 to 10 nm and lateral dimensions of up to a few micrometers (KHARE et al., 2015; ROUXINOL et al., 2010). The MLG powder was dispersed in an ultrasonic bath for a 2-hour period in deionized water. After this, the MLG dispersion in water was added to the plaster through a mixing process. It is important to mention that the amount of water used to disperse the MLG was deducted from the amount of kneading water, thus keeping the water/plaster factor constant at 0.5.

2.2 SPECIMEN PREPARATION

Samples were made in six different MLG concentrations according to the methodology proposed by the Brazilian Standard ABNT/NBR-12129:2019 ‘‘Gypsum for civil construction - Determination of mechanical properties”. The MLG percentages studied were 0%, that is, the Control Group (CG), 0.0150% (150MLG), 0.0175% (175MLG), 0.020% (200MLG) and 0.025% (250MLG) in relation to the gypsum plaster’s powder mass. For all samples the water/plaster ratio (w/p) was 0.5. The MLG dispersed in deionized water (see section 2.1) was incorporated into the kneading water, adding a w/p factor of 0.5 at a temperature of 25 ^{0}C. Cubic specimens with an edge of 50 mm were obtained for carrying out the compression tests in accordance with the ABNT/NBR Standard-12129:2019. Regarding the tensile strength tests by diametral compression (see ABNT/NBR Standard-7222:2011), the specimens were made in a cylindrical shape with a diameter of 5 cm and a height of 10 cm. The samples were obtained at room temperature, demolded after 3 h, and stored at room temperature and humidity until the rupture date.

2.3 MORPHOLOGICAL ANALYSIS

The morphological properties of gypsum plaster containing different amounts of MLG were verified by scanning electron microscopy, using a FEG-SEM JEOL 7001F microscope (TESCAN/VEGA-3) equipped with an EDX Oxford element detector. The

optical microscopy technique was used to verify the distribution of MLG particles in the plaster paste using the Nova Model 156-T equipment. The morphological properties were also verified by optical microscopy.

2.4 STRUCTURAL ANALYSIS

The chemical composition analyses were performed by Raman spectroscopy, using the LabRAM HR Evolution – HORIBA equipment, with an excitation source of 532 nm and power adjusted to 2.5 mW. Fourier transform infrared spectroscopy (FTIR) was used to investigate the chemical structure of the composites prepared in this study. The FTIR spectra were obtained with an Agilent Cary 640 spectrometer using the diffuse reflection mode with the Pike Veemax II accessory. The spectra were performed in the range from 4000 to 500 cm^{-1}, with a resolution of 4 cm^{-1}. The samples used in the FTIR analyses were obtained from fragments taken from the interior of mechanically tested specimens that were over 120 days old. X-ray diffraction (XRD) analyses were performed using a Shimadzu XRD-6100 diffractometer in the range of -6º to 80º (2θ) with a scan speed of 1º/min.

2.5 NORMAL CONSISTENCY AND SETTING START AND END TIME ANALYSES

Normal consistency and setting start and end time analyses were performed according to the ASTM-C472 standard - "Standard Test Methods for Physical Testing of Gypsum, Gypsum Plasters and Gypsum Concrete". Hydration curves were obtained from temperature measurements of samples placed in an adiabatic box. For this, a system composed of a thermocouple and Arduino was used, and the measurements took place over a 3-hour period.

2.6 MASS LOSS TESTS

The mass loss tests were carried out with the aim of verifying the influence of MLG's hydrophobic properties on the plaster's resistance to water. For this, the samples were submerged in distilled water at room temperature for a 2 h period. At first, the samples were dried in an oven at 80 ^{0}C for 24 h. After this procedure, the masses were measured using a BEL Engineering Model M214Ai analytical balance and submerged in distilled water yet again. After 2 h of submersion, the samples were dried again in an oven at 80 °C until they stabilized. After the stabilization of their masses and at room

temperature, the difference between the initial and final dry masses was measured in percentage.

2.7 TENSILE AND COMPRESSIVE STRENGTH TESTS

The compressive and tensile strength tests were performed using a digital servo-hydraulic press (Contenco/HD200T), with a maximum load capacity of 2000 kN. The compression tests were determined following the protocols described by the Regulatory Agency ABNT/NBR-12129:2019 “Gypsum plaster for civil construction - Determination of mechanical properties", using a loading rate of 0.2 ± 0.1 MPa/s; The tensile strength was measured following the procedures described by ABNT/NBR7222:2011 "Concrete and mortar - Determination of tensile strength by diametral compression of cylindrical specimens" with a loading rate of 0.05 ± 0.02 MPa /s. Compressive strength was analyzed at ages 1, 3 and 7 days and tensile strength at ages 1 and 7 days, respectively. Following the guidance of adopted standards, at least 3 specimens were tested for each batch in each age group, and the resistance considered was the average of these samples. The maximum variation allowed between each sample’s individual mechanical strength and the average of the results was 15%.

3 RESULTS & DISCUSSIONS

3.1 MORPHOLOGICAL ANALYSIS

Figures 1 (a-c) present the images obtained via optical microscopy for the reference samples (CG), 225MLG and 250MLG, respectively. It should be noted that there was no significant difference in the morphological structure of the surfaces with the magnifications used.

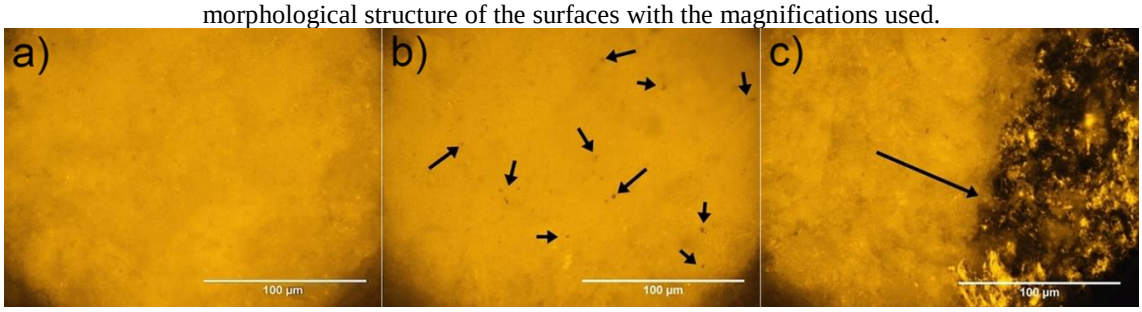

Source: Images obtained by optical microscopy (magnification 500x), a) CG sample, b) 225MLG sample with good dispersion, c) 250MLG sample with agglomeration. Black arrows indicate MLG and agglomerations, respectively.

In regard to the MLG distribution, it is possible to verify a tendency for the flakes to agglomerate, as observed in the 250MLG sample, even when using a low MLG weight

concentration. These observations were indicated even after performing a good mechanical mixing of the pastes during the molding process of the specimens.

Figure 2. Images obtained via SEM with a magnification of 5 kx, (a) representative MLG flake, (b) CG Sample, (c) 225MLG Sample and (d) 250MLG Sample.

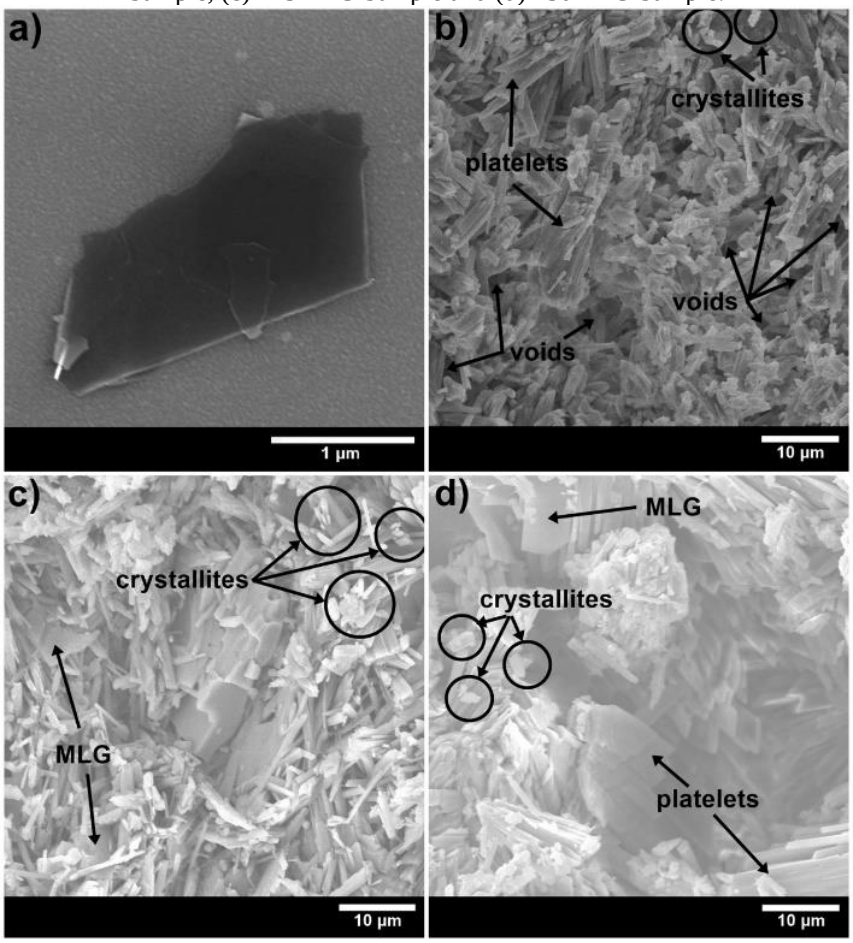

Figures 2 (a - d) show the micrographs obtained via SEM for a representative MLG flake and for the CG, 225MLG and 250MLG samples, respectively. The MLG flake had a structure with no surface defects, presenting micrometric dimensions and a low number of superimposed layers (1 to 10 layers) (see **Figure 2 (a)**). As reported in the literature, the absence of defects in MLG flakes provides good mechanical (BALDIN et al., 2021; SILVA et al., 2017), thermal (NATIVIDADE et al., 2019) and electrical (AUGUSTO et al., 2018; MOURA et al., 2021) properties, promoting a wide range of applications.

Regarding the gypsum mortar samples, there is a certain difference both in the crystal sizes and the porosity of the samples. The CG sample (see **Figure 2 (b)**) had an average size of 1.46 µm and a length of 5.45 µm. The 225MLG sample (**Figure 2 (c)**)

showed a higher density of crystals with smaller unit dimensions (average diameter of 0.95 µm and length 4.94 µm). As reported in the literature (HINCAPIE; CINCOTTO, 1997;MOGHADAM; MIRZAEI, 2020), the increase in crystal density is directly related to the improvement of mechanical properties (GARTNER, 2009) and a decrease in water absorption (MOGHADAM; MIRZAEI, 2020). The 250MLG sample (**Figure 2 (d)**) presented crystals with similar diameters to the GC (~1.3 µm) and an average length of 8.23 µm.

3.2 STRUCTURAL CHARACTERIZATION

3.2.1 Xrd Results

The XRD technique was used to characterize the CG, 150MLG, 175MLG, 200MLG, 225MLG and 250MLG samples. The experimental and simulated spectra are shown in **Figure 3**. The simulated spectrum corresponds to the $CaSO_4 \cdot 2H_2O$ phase (ATOJI; RUNDLE, 1958; BOEYENS; ICHHARAM, 2002) and presents a monoclinic structure (space group C12/c1). As can be seen in **Figure 3**, the gypsum phase is present in all specimens studied. All peaks present can be related to the monoclinic phase, with the exception of a single reflection observed at $2\theta \sim 25^{o}$ for samples containing MLG. This peak was indexed as belonging to the □-$CaSO_4$ phase (HAWTHORNE; FERGUSON, 1975). Transformations between these phases are common in gypsum hydration reactions (RITTERBACH; BECKER, 2020). However, as this phase is not present in the control sample (CG), it can be suggested that the presence of MLG may interfere with the hydration mechanisms of the gypsum plaster in question. As the MLG concentrations used in the present study are considerably low and below the detection limit of the equipment used, no contribution from this nanostructure was observed in the diffractograms obtained. No variation in the lattice parameters was observed for the $CaSO_4 \cdot 2H_2O$ phase, which leads to the conclusion that there is no chemical reaction between this phase and the MLG, which is only acting as an aggregate to the composite material, reinforcing the FTIR results presented in **Figure 5** to be discussed later.

Figure 3. X-ray diffractograms for the control group (CG) and for the composites containing MLG. The spectrum also shows the simulated diffractogram for the gypsum phase ($CaSO_4 \cdot 2H_2O$). The black arrow shows the presence of the β-$CaSO_4$ phase.

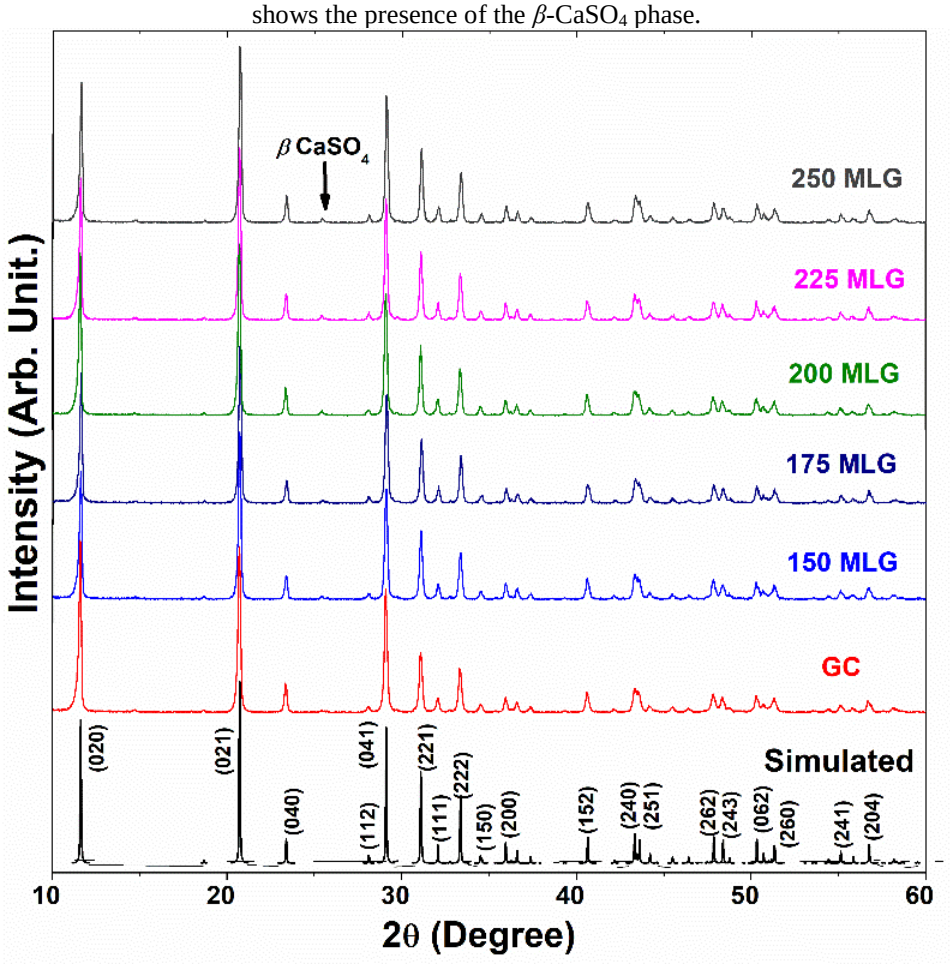

3.2.2 Raman Results

Figure 4 illustrates typical Raman spectra for a natural graphite crystal and MLG particulates. For natural graphite, the band related to the G mode at 1590 cm^{-1} is related to the tangential stretching of the C-C bonds in graphitic materials (MORETO et al., 2022). The band around 1355 cm^{-1} (D-mode) is associated with the breathing mode of the sp^2 carbon present in the hexagonal crystal structure and related to the presence of structural disorder (AUGUSTO et al., 2018). The absence of peak D in the graphite spectrum is associated with high crystallinity and a low number of defects in this sample. The other characteristic bands D, G, D', D+D", 2D, D+D' and 2D' are also seen in **Figure 4**. The 2D band at ~2750 cm^{-1} as well as D+D", D+ D' and 2D' around ~2450 cm^{-1}, ~2960 cm^{-1}, and ~3250 cm^{-1} are derived from two-photon processes and associated with defect-free structures (CARVALHO et al., 2015; FERRARI; BASKO, 2013; MAFRA et al., 2007; THOMSEN; REICH, 2000; VENEZUELA; LAZZERI; MAURI, 2011). The presence of the D band in the spectrum related to the MLG sample indicates the presence

of defects in its structure originating from the exfoliation process and can be associated with edge defects (MOURA et al., 2021).

Figure 4. Raman spectra for a large natural graphite specimen and MLG powder. The inset illustrates the photos of a natural graphite crystal and the MLG powder herein used.

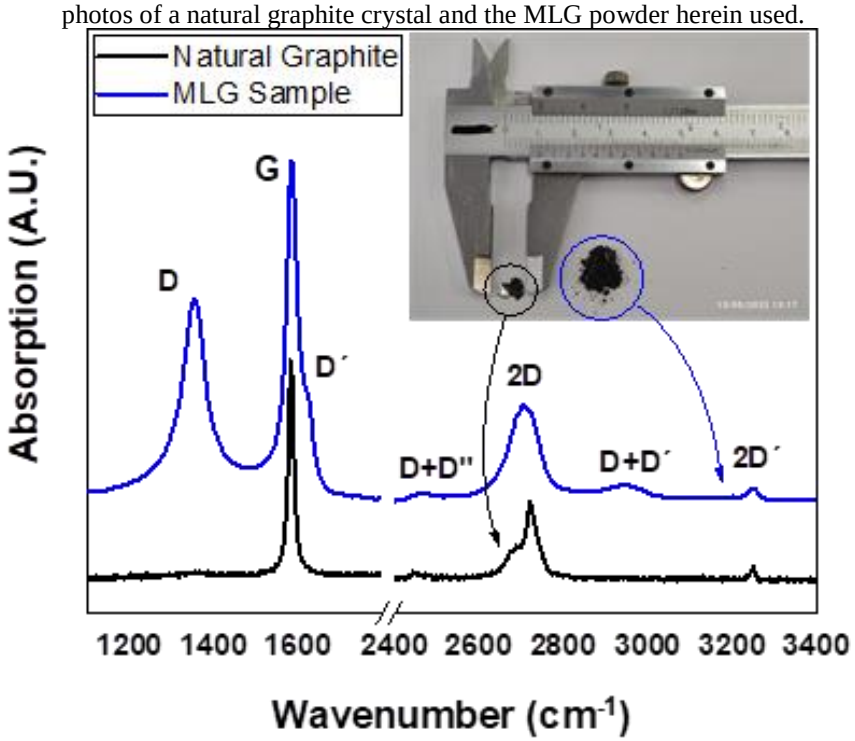

3.2.3 Ftir Results

The FTIR spectra for the CG and CG containing MLG, in the range from 4000 to 500 cm^{-1} are presented in **Figure 5**. A very high similarity between the chemical structures of the studied samples is observed through the spectra, indicating that the addition of graphene did not interfere with the specimens' chemical structures. In addition, bands related to the sulfate group are noted and centered at 1250 cm^{-1}, 1005 cm^{-1}, 600 cm^{-1}, 670 cm^{-1}, 450 cm^{-1} and 420 cm^{-1} (ADLER; KERR, 1965; ANBALAGAN et al., 2009; BLANEY; MCCORD, 1995; COOPER; MUSTARD, 2002). The bands centered at 3620 cm^{-1} and 3640 cm^{-1} (ANBALAGAN et al., 2009; RYSKIN, 1974), and at 1620 cm^{-1} (SEIDL; KNOP; FALK, 1969) and 3200 cm^{-1} refer to water. Low intensity bands centered at 1460, 2850 and 2915 cm^{-1} are associated with C-H (ANBALAGAN et al., 2009), identified in the experimental bands possibly by the presence of MLG. Therefore, from a chemical point of view, the samples are little influenced by the addition of MLG.

Figure 5. FTIR spectra for the CG and the CG containing MLG, in the ranges of (a) 4000 to 2000 cm^{-1} and (b) 2000 to 500 cm^{-1}.

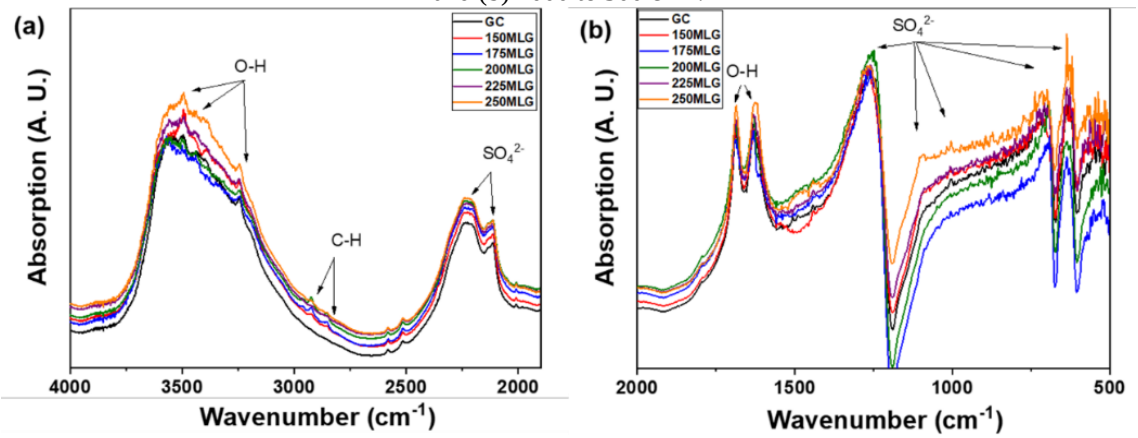

3.3 CONSISTENCY, SETTING TIMES AND CALORIMETRY RESULTS

Table 1 presents the values obtained for the initial and final setting times for the CG, 150MLG, 175MLG, 200MLG, 225MLG and 250MLG samples, respectively. As can be seen, except for the 225MLG sample, all the others had lower initial (T1) and final (T2) setting times than the CG. As reported in other studies (HAO et al., 2021; LEWRY; WILLIAMSON, 1994), the decrease in initial setting time is indicative of greater nucleation, greater crystalline activity and greater intensity of reactions mainly in peripheral areas (region where the needle of the Vicat device is inserted when the setting times are verified). Thus, the more crystallization nuclei, the greater the number of crystals and the smaller their unitary dimensions (UCHYMIAK et al., 2008), that is, the greater their long-term crystalline density.

Table 1. Initial and final setting times for the samples considered in the present work.

Setting times (h:m:s)			
Samples	**Initial setting time (T1)**	**Final setting time (T2)**	**T2-T1**
CG	00:16:35	00:21:20	00:04:45
150MLG	00:11:40	00:17:28	00:05:47
175MLG	00:13:05	00:21:15	00:08:10
200MLG	00:11:30	00:17:20	00:05:50
225MLG	00:19:35	00:26:20	00:06:45
250MLG	00:12:23	00:16:45	00:04:22

The 225MLG sample presented higher initial and final setting times than that of the CG, indicating slower crystallization, which can be explained by the gypsum plaster solubility related to the hydration temperature. Simply put, the amount of energy that is injected into the system ends up acting as a catalyst for the hydration reactions, optimizing the material's crystallization rate and increasing the plaster solubility (COQUARD et al.,

1994; MARSHALL; SLUSHER, 1966). However, this phenomenon is observed up to a temperature of approximately 50 °C. From this temperature value, the solubility decreases. Thus, it is suggested that the 225MLG sample distributed energy to the gypsum plaster paste, allowing for the mobility of the Ca^{+2} SO_4^{2-} ions, delaying the setting and the growth of crystals.

It is interesting to observe that all experimental samples (except 250MLG) presented a greater interval between the initial and final of the setting time. The early initial setting time factor may be related to increased nucleation, and the prolonged T2-T1 interval to slower crystal growth. The probable mechanisms regarding the crystal growth time as well as the effects caused on the crystal properties are discussed ahead.

Figure 6 shows the hydration curve for the CG, 175MLG, 225MLG and 250MLG samples, respectively. It is noted that the 225MLG and 250MLG samples presented lower temperature values in the calorimetric analyses, suggesting that the MLG acts as an energy sink and, in fact, graphene acts as a good thermal conductor (DEY et al., 2016). Considering the post final setting time, samples containing MLG present higher temperature values, between 60-65 ºC, indicating greater crystalline activity in the period, which reinforces an idea of crystallization over longer periods of time. It is emphasized that the method has different setting times from the Vicat apparatus method due to the pseudo adiabatic conditions, which change the material's solubility. In this case, the times serve to determine the periods of the curve. The initial setting time considered in the hydration curve concerns the beginning of crystalline nucleation, where the temperature increase is observed due to the exothermic characteristic of the hydration reaction. The final setting time of the curve is defined from the temperature stabilization trend.

Figure 6. Hydration curve for the CG, 175MLG, 225MLG and 250MLG samples.

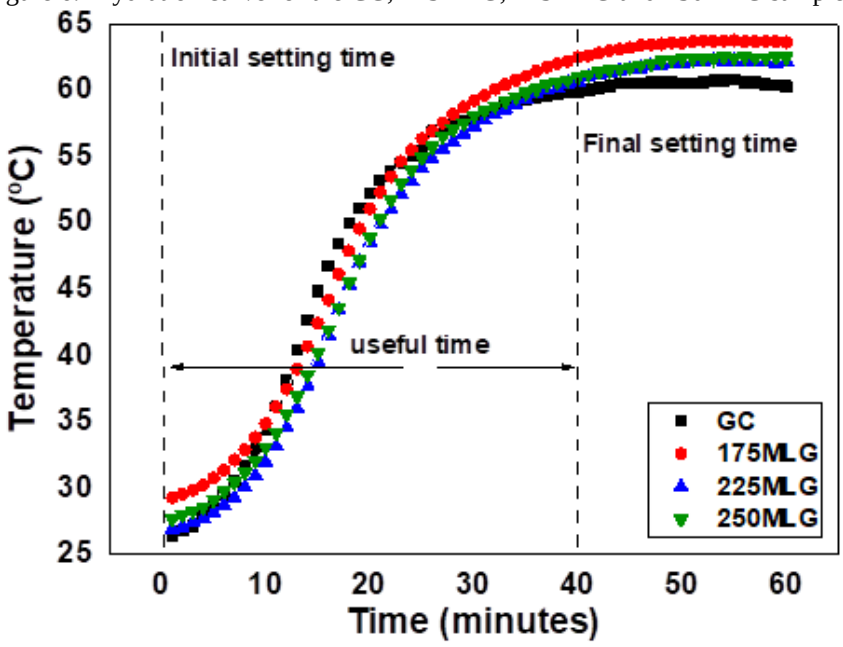

3.4 MASS LOSS BY SUBMERSION IN WATER AND CONSISTENCY

Gypsum plaster is a soluble material, and when exposed to water it tends to incorporate it, weakening the bonds between the crystals by capillary pressure. The more intense the interactions between the crystal surfaces and the lower the porosity of the solid body, the more resistant to the effect of water the material will be (MOGHADAM; MIRZAEI, 2020; SINGH; GARG, 1996). The plaster hydration process during the so-called induction period also influences the water tolerance of the hardened material (KANNO, 2010). It was observed that the higher the graphene dosage used in the plaster paste, the lower the average mass loss (see **Figure 7 (a)**). The 250MLG sample lost about 36.4% less mass than the sample made without the additive. It can be suggested that the samples containing MLG present higher crystalline density and greater intergranular interaction than the CG sample, which allowed for less mass loss. Graphene's hydrophobicity can make it difficult for water to penetrate the pores of the plaster and it, therefore, maintains its more aggregated structure than when compared to the reference material, preventing the detachment of material. As for consistency, it was observed that the MLG did not influence the properties of the paste (**Figure 7 (b)**) and all samples presented values close to 20 mm.

Figure 7. (a) Mass loss results by total submersion in water and (b) Consistency results.

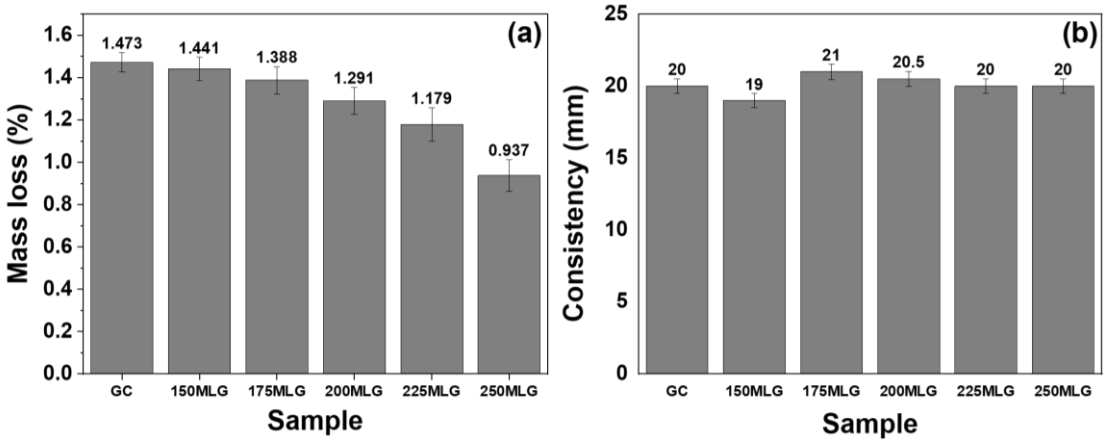

3.5 COMPRESSION AND TENSILE TESTS RESULTS

The compressive and tensile strength results performed at the age of 1, 3 and 7 days are shown in **Table 2** and **Figure 8**, respectively. From the results of compressive strength, it is noted that the amount of graphene in the proportion of 0.015% (150MLG) does not affect the plaster's crystallization process and, consequently, its compressive strength at the ages considered. The values presented in **Figure 8 (a)** are consistent with the results obtained in the fresh state of the plaster samples, which indicated a similar behavior between the 150MLG and the CG samples. At the MLG dosage of 0.0175% (sample 175MLG), a modest influence of the graphene on the plaster's mechanical behavior can be suggested.

At the first age tested, the 175MLG, 200MLG and 225MLG samples showed lower performance than the CG sample. In the SEM images (**Figure 2**), one can observe crystals with smoother surfaces and well-defined corners in the samples containing MLG. These characteristics may indicate that the crystals were formed over a longer period, providing higher unit density, which contributes to the final mechanical strength (BARBOSA; FERRAZ; SANTOS, 2014). On the other hand, crystals formed in short periods of time are porous and have a spongy appearance (BARBOSA; FERRAZ; SANTOS, 2014), similar to the crystals in the CG reference sample (**Figure 2 (a)**).

Table 2. Average axial compressive strength (MPa) results.

Age (days)	GC	150MLG	175MLG	200MLG	225MLG	250MLG
1	2.87±0.14	2.87±0.14	2.47±0.12	2.37±0.12	2.20±0.11	3.35±0.17
3	2.83±0.14	2.90±0.15	3.07±0.15	3.45±0.17	2.45±0.12	3.33±0.17
7	3.03±0.15	3.03±0.15	3.17±0.16	6.73±0.34	5.10±0.26	5.37±0.27

In this context, it can be suggested that the performances observed in the first age are due to the CG's higher crystallization rate at that moment, since its crystals developed in a shorter period. It can also be suggested that the heat distribution promoted by graphene may have affected the plaster's degree of solubility, since the temperature changes the setting time of the material, and above 50º C, the solubility ratio of the hemihydrate and dihydrate decrease, causing a delay in setting and crystallization time, and increasing the mobility of calcium and sulfate ions as the temperature of the medium increases (COQUARD et al., 1994; HULETT; ALLEN, 1902; MARSHALL; SLUSHER, 1966). Resumption of strength gains is observed in the 3-day-old experimental samples, which indicates long-term crystalline activity, which is consistent with the hydration curve (Figure 6), where it is possible to observe higher temperatures after the setting end time in samples containing MLG. As for the results at 7 days, **Figure 8 (b)** shows a performance gain for the 200MLG sample, that is, an increase of about 122% compared to the CG sample at the same age. The 225MLG sample showed a performance 38.13% higher than the CG at 7 days of age, and the lowest performance among all the samples at the first age tested (23.25% lower than the CG). These results are consistent with the setting time observed for this sample, since the 225MLG experimental range was the only one to present higher setting times than the control sample, indicating slower crystallization.

The 250MLG sample presented higher compressive strength than the others at the age of 1 day. This may have occurred due to the influence of the agglomerated graphene, as can be seen in the optical microscopy (**Figure 1 (c)**). It can be inferred that the graphene agglomeration may have acted as a crystal, which helped to gain strength at the age of 1 day, and also that the heat dissipation effects promoted by the MLG were attenuated due to poor dispersion. The 250MLG sample presented a performance 76.92% superior to the CG at 7 days, a performance inferior to the 225MLG sample. It is believed that the MLG agglomeration tendency affected the results, since the dispersion of MLG in the paste was compromised.

Figure 8. (a) Axial compressive strength ($\sigma_{C)}$ for plaster pastes with different MLG doses as a function of time (upper graph) and (b) relative variation of axial compressive strength for the sample without MLG (σ_{co}).

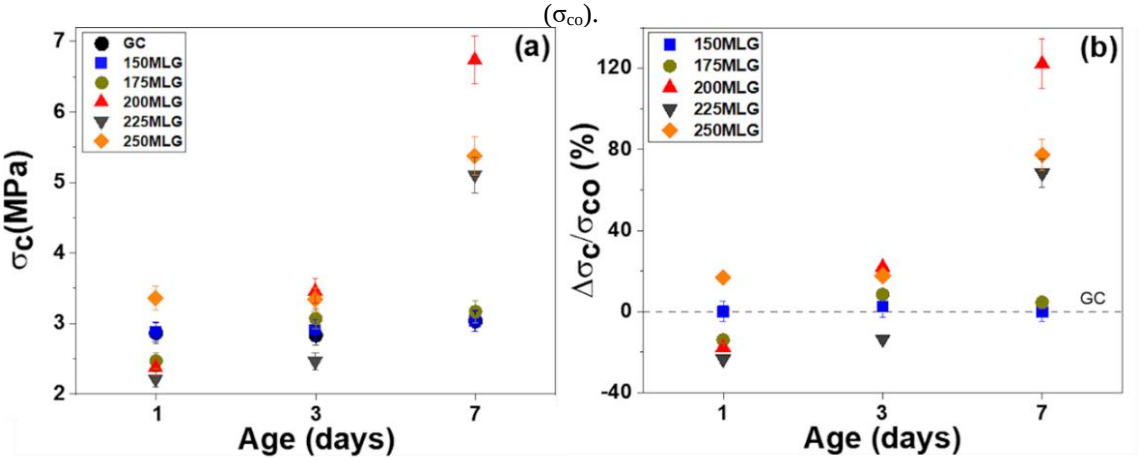

Table 3. Average tensile strength results by diametral compression (MPa).

Age (days)	GC	150MLG	175MLG	200MLG	225MLG	250MLG
1	1.6±0.08	1.7±0.09	1.75±0.09	1.55±0.08	1±0.05	1.7±0.09
7	1.6±0.08	1.6±0.08	3.3±0,17	3.55±0.18	3,1±0.16	3.03±0.15

In regard to tensile strength, it is observed that in the first age of 1 day, all ranges performed similar results, except for the 225MLG sample, which is in accordance with the idea of slow crystallization. It can be seen from the graph in **Figure 9 (a)** that the 150MLG sample presented results practically identical to the CG reference sample. The same occurred for the compression and consistency results, which reinforces the theory that at this dosage the MLG does not significantly influence the material 's fluidity and mechanical properties. At 175MLG, different from what was observed in the compression results, there is a performance 106.25% superior to that of the CG at 7 days (**Figure 9 (b)**), indicating that this MLG dosage acted as a tensile strength enhancer at this age. Although the compression performance was not significantly higher when comparing the CG to the 175MLG, a reduction in setting times was observed, indicating changes in crystalline activities.

Comparing the results obtained here with those of Jara et al. (JARA; PÉREZ; YEPES, 2020; JARA; YEPES; PÉREZ, 2021), the MLG insertion in the concentrations studied here proved to be very promising. Jara et al. report a 12.8% improvement in compressive strength for a 0.1% graphene concentration. Our results indicate values above 122% for a 0.2% MLG concentration without evidence of particle agglomeration as well as maintaining the structural and chemical integrity of the gypsum mortar samples,

guaranteeing the same morphological characteristics. Regarding the tensile analyses, Jara et al. report an increase of about 22% for the flexural strength at the 0.010% graphene concentration while our results indicate an increase of 121% for the 0.020% MLG concentration. With the exception of the 0.150% MLG sample, all the others showed tensile strength values close to 7 days, indicating that this property is more attractive for the use of MLG as an additive.

Figure 9. (a) Tensile strength by diametral compression (σ_T) for plaster pastes with different MLG doses as a function of time (upper graph) and (b) relative variation in relation to the sample without MLG (σ_{TO}).

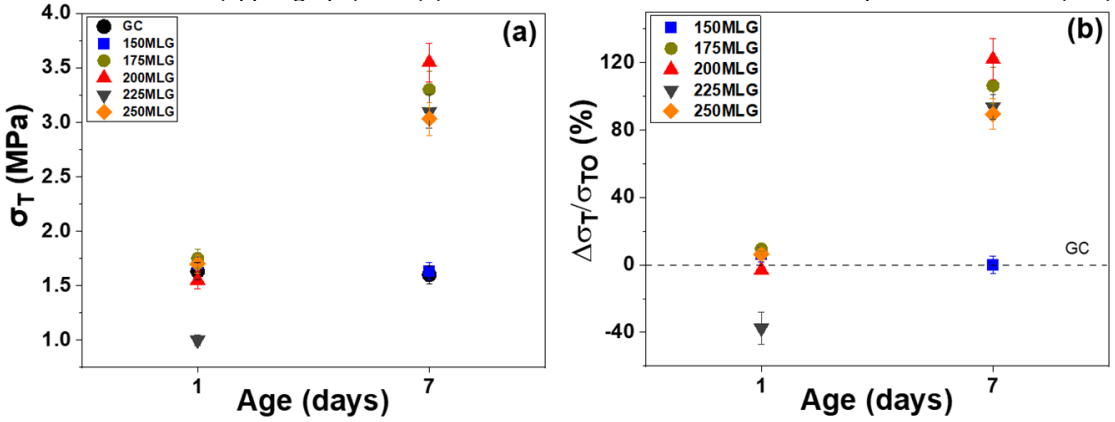

Thus, the 200MLG sample range demonstrated, at 7 days, tensile performance about 120% superior to the CG as shown in **Figure 9 (b)**. This was also observed in the axial compression results. The 225MLG and 250MLG samples showed similar resistance at 7 days, being higher than the CG sample and lower than the 200MLG sample.

4 CONCLUSIONS

The use of graphene with gypsum plaster proved to be efficient, optimizing its mechanical tensile and compressive strengths by about 120% at 7 days at a dosage of 0.02% in relation to the mass of the gypsum plaster powder. In comparison to the sample without graphene, it was observed that: *i*) there were no significant changes in consistency of the samples; *ii*) the setting times were affected, showing an increase for the samples with graphene; *iii*) samples with graphene lost less mass when submerged in water; *iv)* a low intensity peak attributed to the β-$CaSO_4$ phase was observed in the XRD diffractograms in the samples containing MLG. This was probably due to the internal heat transfer promoted by this nanostructure. Thus, it is likely that the graphene promoted internal heat dissipation, allowing for a greater degree of hydration in the peripheral regions of the paste, promoting greater crystalline density and crystals with better

morphological properties. The MLG may have also acted as a crystallization nucleus, increasing the saturation of the Ca^{2+} ions through reactivity with the graphene surface. The MLG used, obtained from natural graphite, has a low cost, a low production time and is used in very small quantities. Thus, from an additive of low added value, it is possible to encourage the use of gypsum plaster on a larger scale as an alternative to cement-based compounds, contributing to sustainability by reducing the energy consumption and gas emissions produced by the cement industry.

REFERENCES

ADLER, H. H.; KERR, P. F. Variations in infrared spectra, molecular symmetry and site symmetry of sulfate minerals. **American Mineralogist**, [s.l.], v. 50, nº 1–2, p. 132–147, 1965. ISSN: 0003-004X.

ANBALAGAN, G. et al. Infrared, optical absorption, and EPR spectroscopic studies on natural gypsum. **Vibrational Spectroscopy**, [s.l.], v. 50, nº 2, p. 226–230, 2009. ISSN: 09242031, DOI: https://doi.org/10.1016/j.vibspec.2008.12.004.

ATOJI, M.; RUNDLE, R. E. Neutron Diffraction Study of Gypsum, $CaSO_4 2H_2O$. **The Journal of Chemical Physics**, [s.l.], v. 29, nº 6, p. 1306–1311, 1958. ISSN: 0021-9606, DOI: https://doi.org/10.1063/1.1744713.

AUGUSTO, G. de S. et al. Flexible metal-free supercapacitors based on multilayer graphene electrodes. **Electrochimica Acta**, [s.l.], v. 285, p. 241–253, 2018. ISSN: 00134686, DOI: https://doi.org/10.1016/j.electacta.2018.07.223.

BALDIN, V. et al. Effect of Graphene Addition in Cutting Fluids Applied by MQL in End Milling of AISI 1045 Steel. **Lubricants**, [s.l.], v. 9, nº 7, p. 70, 2021. ISSN: 2075-4442, DOI: https://doi.org/10.3390/lubricants9070070.

BARBOSA, A. A.; FERRAZ, A. de V.; SANTOS, G. A. Caracterização química, mecânica e morfológica do gesso obtido do pólo do Araripe. **Cerâmica**, [s.l.], v. 60, nº 356, p. 501–508, 2014. ISSN: 0366-6913, DOI: https://doi.org/10.1590/S0366-69132014000400007.

BLANEY, D. L.; MCCORD, T. B. Indications of sulfate minerals in the Martian soil from Earth-based spectroscopy. **Journal of Geophysical Research**, [s.l.], v. 100, nº E7, p. 14433, 1995. ISSN: 0148-0227, DOI: https://doi.org/10.1029/95JE00224.

BOEYENS, J. C. A.; ICHHARAM, V. V. H. Redetermination of the crystal structure of calcium sulphate dihydrate, $CaSO_4 \cdot 2H_2O$. **Zeitschrift für Kristallographie - New Crystal Structures**, [s.l.], v. 217, nº JG, p. 9–10, 2002. ISSN: 2197-4578, DOI: https://doi.org/10.1524/ncrs.2002.217.jg.9.

BORRACHERO, M. V. et al. The use of thermogravimetric analysis technique for the characterization of construction materials. **Journal of Thermal Analysis and Calorimetry**, [s.l.], v. 91, nº 2, p. 503–509, 2008. ISSN: 1388-6150, DOI: https://doi.org/10.1007/s10973-006-7739-3.

BROWNSON, D. A. C.; KAMPOURIS, D. K.; BANKS, C. E. Graphene electrochemistry: fundamental concepts through to prominent applications. **Chemical Society Reviews**, [s.l.], v. 41, nº 21, p. 6944, 2012. ISSN: 0306-0012, DOI: https://doi.org/10.1039/c2cs35105f.

CARVALHO, F. H. O. et al. Synthesis of Carbon Nanostructures Near Room Temperature Using Microwave PECVD. **Materials Research**, [s.l.], v. 18, nº 4, p. 860–866, 2015. ISSN: 1516-1439, DOI: https://doi.org/10.1590/1516-1439.005315.

CHAROLA, A. E.; PÜHRINGER, J.; STEIGER, M. Gypsum: a review of its role in the deterioration of building materials. **Environmental Geology**, [s.l.], v. 52, nº 2, p. 339–352, 2007. ISSN: 0943-0105, DOI: https://doi.org/10.1007/s00254-006-0566-9.

CHEN, D.; TANG, L.; LI, J. Graphene-based materials in electrochemistry. **Chemical Society Reviews**, [s.l.], v. 39, nº 8, p. 3157, 2010. ISSN: 0306-0012, DOI: https://doi.org/10.1039/b923596e.

CHUNG, D. D. L. Carbon materials for structural self-sensing, electromagnetic shielding and thermal interfacing. **Carbon**, [s.l.], v. 50, nº 9, p. 3342–3353, 2012. ISSN: 00086223, DOI: https://doi.org/10.1016/j.carbon.2012.01.031.

COOPER, C. D.; MUSTARD, J. F. Spectroscopy of Loose and Cemented Sulfate-Bearing Soils: Implications for Duricrust on Mars. **Icarus**, [s.l.], v. 158, nº 1, p. 42–55, 2002. ISSN: 0019-1035, DOI: https://doi.org/10.1006/icar.2002.6874.

COQUARD, P. et al. Hardness, elasticity modulus and flexion strength of dry set plaster. **Journal of Materials Science**, [s.l.], v. 29, nº 17, p. 4611–4617, 1994. ISSN: 0022-2461, DOI: https://doi.org/10.1007/BF00376285.

DEY, A. et al. Plasma engineering of graphene. **Applied Physics Reviews**, [s.l.], v. 3, nº 2, p. 21301, 2016. ISSN: 1931-9401, DOI: https://doi.org/10.1063/1.4947188.

FERRARI, A. C.; BASKO, D. M. Raman spectroscopy as a versatile tool for studying the properties of graphene. **Nature Nanotechnology**, [s.l.], v. 8, nº 4, p. 235–246, 2013. ISSN: 1748-3387, DOI: https://doi.org/10.1038/nnano.2013.46.

FREIRE, M. T. et al. Restoration of ancient gypsum-based plasters: Design of compatible materials. **Cement and Concrete Composites**, [s.l.], v. 120, p. 104014, 2021. ISSN: 09589465, DOI: https://doi.org/10.1016/j.cemconcomp.2021.104014.

GARTNER, E. M. Cohesion and expansion in polycrystalline solids formed by hydration reactions — The case of gypsum plasters. **Cement and Concrete Research**, [s.l.], v. 39, nº 4, p. 289–295, 2009. ISSN: 00088846, DOI: https://doi.org/10.1016/j.cemconres.2009.01.008.

GDOUTOS, E. E. et al. Advanced cement based nanocomposites reinforced with MWCNTs and CNFs. **Frontiers of Structural and Civil Engineering**, [s.l.], v. 10, nº 2, p. 142–149, 2016. ISSN: 2095-2430, DOI: https://doi.org/10.1007/s11709-016-0342-1.

GERALDO, R. H. et al. Gypsum plaster waste recycling: A potential environmental and industrial solution. **Journal of Cleaner Production**, [s.l.], v. 164, p. 288–300, 2017. ISSN: 09596526, DOI: https://doi.org/10.1016/j.jclepro.2017.06.188.

GONG, K. et al. Reinforcing Effects of Graphene Oxide on Portland Cement Paste. **Journal of Materials in Civil Engineering**, [s.l.], v. 27, nº 2, p. A4014010, 2015. DOI: https://doi.org/10.1061/(ASCE)MT.1943-5533.0001125.

HAO, J. V. Preparation of high-performance building gypsum by calcining FGD gypsum adding CaO as crystal modifier. **Construction and Building Materials**, [s.l.], v. 306, p. 124910, 2021. ISSN: 09500618, DOI: https://doi.org/10.1016/j.conbuildmat.2021.124910.

HAWTHORNE, F. C.; FERGUSON, R. B. Anhydrous sulphates; II, Refinement of the crystal structure of anhydrite. **The Canadian Mineralogist**, [s.l.], v. 13, nº 3, p. 289–292, 1975. ISSN: 0008-4476.

HINCAPIE, A. M.; CINCOTTO, M. A. Efeito de retardadores de pega no mecanismo de hidratação e na microestrutura do gesso de construção. **Ambiente Construído**, [s.l.], v. 1, nº 2, p. 7–16, 1997. ISSN: 1415-8876.

HOU, L. et al. Effect of nanoparticles on foaming agent and the foamed concrete. **Construction and Building Materials**, [s.l.], v. 227, p. 116698, 2019. ISSN: 0950-0618, DOI: https://doi.org/DOI: https://doi.org/10.1016/j.conbuildmat.2019.116698.

HULETT, G. A.; ALLEN, L. E. The Solubility of Gypsum. **Journal of the American Chemical Society**, [s.l.], v. 24, nº 7, p. 667–679, 1902. ISSN: 0002-7863, DOI: https://doi.org/10.1021/ja02021a007.

ISAIA, G. C.; GASTALDINI, A. L. G. Environmental and economic perspectives of concrete with high mineral addition content: a case study. **Ambiente Construído**, [s.l.], v. 4, nº 2, p. 19–30, 2004. ISSN: 1415-8876.

JARA, L. M. S.; PÉREZ, J. J. P.; YEPES, J. A. F. Study of compressive strength of gypsum with graphene addition. **Cement Wapno Beton**, [s.l.], v. 25, nº 3, p. 232–241, 2020. ISSN: 1425-8129, DOI: https://doi.org/10.32047/CWB.2020.25.3.6.

JARA, L. M. S.; YEPES, J. A. F.; PÉREZ, J. J. P. Analysis of the Resistance to Bending of Gypsum with Added Graphene. **Coatings**, [s.l.], v. 11, nº 6, p. 650, 2021. ISSN: 2079-6412, DOI: https://doi.org/10.3390/coatings11060650.

KHARE, R. T. et al. Enhanced field emission of plasma treated multilayer graphene. **Applied Physics Letters**, [s.l.], v. 107, nº 12, p. 123503, 2015. ISSN: 0003-6951, DOI: https://doi.org/10.1063/1.4931626.

KORTE, A. C. J.; BROUWERS, H. J. H. Calculation of thermal conductivity of gypsum plasterboards at ambient and elevated temperature. **Fire and Materials**, [s.l.], v. 34, nº 2, p. 55–75, 2010. DOI: https://doi.org/DOI: https://doi.org/10.1002/fam.1009.

LEE, C. et al. Measurement of the Elastic Properties and Intrinsic Strength of Monolayer Graphene. **Science**, [s.l.], v. 321, nº 5887, p. 385–388, 2008. ISSN: 0036-8075, DOI: https://doi.org/10.1126/science.1157996.

LEWRY, A. J.; WILLIAMSON, J. The setting of gypsum plaster. **Journal of Materials Science**, [s.l.], v. 29, nº 23, p. 6085–6090, 1994. ISSN: 1573-4803, DOI: https://doi.org/10.1007/BF00354546.

LOTA, G. et al. Improvement of the structural and chemical properties of a commercial activated carbon for its application in electrochemical capacitors. **Electrochimica Acta**, [s.l.], v. 53, nº 5, p. 2210–2216, 2008. ISSN: 00134686, DOI: https://doi.org/10.1016/j.electacta.2007.09.028.

MACHUNO, L. G. B. et al. Multilayer Graphene Films Obtained by Dip Coating Technique. **Materials Research**, [s.l.], v. 18, nº 4, p. 775–780, 2015. ISSN: 1516-1439, DOI: https://doi.org/10.1590/1516-1439.005415.

MAFRA, D. L. et al. Determination of LA and TO phonon dispersion relations of graphene near the Dirac point by double resonance Raman scattering. **Physical Review B**, [s.l.], v. 76, nº 23, p. 233407, 2007. ISSN: 1098-0121, DOI: https://doi.org/10.1103/PhysRevB.76.233407.

MARSHALL, W. L.; SLUSHER, R. Thermodynamics of Calcium Sulfate Dihydrate in Aqueous Sodium Chloride Solutions, 0-110°1,2. **The Journal of Physical Chemistry**, [s.l.], v. 70, nº 12, p. 4015–4027, 1966. ISSN: 0022-3654, DOI: https://doi.org/10.1021/j100884a044.

MOGHADAM, H. A.; MIRZAEI, A. Comparing the effects of a retarder and accelerator on properties of gypsum building plaster. **Journal of Building Engineering**, [s.l.], v. 28, p. 101075, 2020. ISSN: 23527102, DOI: https://doi.org/10.1016/j.jobe.2019.101075.

MORETO, J. A. et al. The effect of plasma treatment on flexible self-standing supercapacitors composed by carbon nanotubes and multilayer graphene composites. **Journal of Materials Science**, [s.l.], v. 57, nº 19, p. 8779–8799, 2022. ISSN: 0022-2461, DOI: https://doi.org/10.1007/s10853-022-07162-3.

MORSY, M. S.; ALSAYED, S. H.; AQEL, M. Hybrid effect of carbon nanotube and nano-clay on physico-mechanical properties of cement mortar. **Construction and Building Materials**, [s.l.], v. 25, nº 1, p. 145–149, 2011. ISSN: 09500618, DOI: https://doi.org/10.1016/j.conbuildmat.2010.06.046.

MOURA, G. de M. et al. On the physical and electrochemical properties of MLG-based electrode surfaces modified by microwave-assisted reactive plasma. **Materials Science and Engineering: B**, [s.l.], v. 272, p. 115346, 2021. ISSN: 09215107, DOI: https://doi.org/10.1016/j.mseb.2021.115346.

NATIVIDADE, P. S. G. et al. Experimental analysis applied to an evacuated tube solar collector equipped with parabolic concentrator using multilayer graphene-based nanofluids. **Renewable Energy**, [s.l.], v. 138, p. 152–160, 2019. ISSN: 09601481, DOI: https://doi.org/10.1016/j.renene.2019.01.091.

NOVOSELOV, K. S. et al. Electric Field Effect in Atomically Thin Carbon Films. **Science**, [s.l.], v. 306, nº 5696, p. 666–669, 2004. DOI: https://doi.org/10.1126/science.1102896.

PAPAGEORGIOU, D. G.; KINLOCH, I. A.; YOUNG, R. J. Graphene/elastomer nanocomposites. **Carbon**, [s.l.], v. 95, p. 460–484, 2015. ISSN: 00086223, DOI: https://doi.org/10.1016/j.carbon.2015.08.055.

PARVEEN, S.; RANA, S.; FANGUEIRO, R. A Review on Nanomaterial Dispersion, Microstructure, and Mechanical Properties of Carbon Nanotube and Nanofiber Reinforced Cementitious Composites. **Journal of Nanomaterials**, [s.l.], v. 2013, p. 1–19, 2013. ISSN: 1687-4110, DOI: https://doi.org/10.1155/2013/710175.

PERLOVA, E. et al. Nano Filled Façade Plasters to Increase Durability of Building and Structures. **Materials Science Forum**, [s.l.], v. 871, p. 76–83, 2016. ISSN: 1662-9752, DOI: https://doi.org/10.4028/www.scientific.net/MSF.871.76.

RITTERBACH, L.; BECKER, P. Temperature and humidity dependent formation of $CaSO_4 \cdot xH_2O$ (x = 0...2) phases. **Global and Planetary Change**, [s.l.], v. 187, p. 103132, 2020. ISSN: 09218181, DOI: https://doi.org/10.1016/j.gloplacha.2020.103132.

ROSATO, L. et al. Study and evaluation of nano-structured cellulose fibers as additive for restoration of historical mortars and plasters. **Materials Today: Proceedings**, [s.l.], v. 4, nº 7, p. 6954–6965, 2017. ISSN: 22147853, DOI: https://doi.org/10.1016/j.matpr.2017.07.025.

ROUXINOL, F. P. et al. Low contact resistivity and strain in suspended multilayer graphene. **Applied Physics Letters**, [s.l.], v. 97, nº 25, p. 253104, 2010. DOI: https://doi.org/10.1063/1.3528354.

SEIDL, V.; KNOP, O.; FALK, M. Infrared studies of water in crystalline hydrates: gypsum, $CaSO_4 \bullet 2H_2O$. **Canadian Journal of Chemistry**, [s.l.], v. 47, nº 8, p. 1361–1368, 1969. DOI: https://doi.org/10.1139/v69-223.

SENFF, L. et al. Development of multifunctional plaster using nano-TiO_2 and distinct particle size cellulose fibers. **Energy and Buildings**, [s.l.], v. 158, p. 721–735, 2018. ISSN: 03787788, DOI: https://doi.org/10.1016/j.enbuild.2017.10.060.

SILVA, R. A. et al. Enhanced properties of cement mortars with multilayer graphene nanoparticles. **Construction and Building Materials**, [s.l.], v. 149, p. 378–385, 2017. ISSN: 09500618, DOI: https://doi.org/10.1016/j.conbuildmat.2017.05.146.

SINGH, M.; GARG, M. Relationship between mechanical properties and porosity of water-resistant gypsum binder. **Cement and Concrete Research**, [s.l.], v. 26, nº 3, p. 449–456, 1996. ISSN: 00088846, DOI: https://doi.org/10.1016/S0008-8846(96)85032-0.

THOMSEN, C.; REICH, S. Double Resonant Raman Scattering in Graphite. **Physical Review Letters**, [s.l.], v. 85, nº 24, p. 5214–5217, 2000. ISSN: 0031-9007, DOI: https://doi.org/10.1103/PhysRevLett.85.5214.

UCHYMIAK, M. et al. Kinetics of gypsum crystal growth on a reverse osmosis membrane. **Journal of Membrane Science**, [s.l.], v. 314, nº 1–2, p. 163–172, 2008. ISSN: 03767388, DOI: https://doi.org/10.1016/j.memsci.2008.01.041.

VENEZUELA, P.; LAZZERI, M.; MAURI, F. Theory of double-resonant Raman spectra in graphene: Intensity and line shape of defect-induced and two-phonon bands. **Physical Review B**, [s.l.], v. 84, nº 3, p. 35433, 2011. ISSN: 1098-0121, DOI: https://doi.org/10.1103/PhysRevB.84.035433.

WEI, W.; QU, X. Extraordinary Physical Properties of Functionalized Graphene. **Small**, [s.l.], v. 8, nº 14, p. 2138–2151, 2012. ISSN: 16136810, DOI: https://doi.org/10.1002/smll.201200104.